Chapter 8
Shock-Induced Chemistry: Molecular Dynamics and Coarse Grain Modeling

Md Mahbubul Islam, Mathew Cherukara, Edwin Antillon and Alejandro Strachan

Abstract The fast loading rates associated with shockwaves in solids make molecular dynamics (MD) a particularly well-suited tool for their study. This chapter focuses on recent methods to study shock-induced chemistry using all-atom reactive MD and coarse-grained simulations and their application. We describe insight on the formation of hot spots formed following the shock-induced collapse of pores and their transition to a deflagration wave in high energy density materials obtained from large-scale MD simulations using the reactive force field ReaxFF. Experimental validation of such simulations is critical to assess the predictive capabilities of these methods to describe new materials and show how to extract observables from the simulations that can be directly contrasted with experiments. Such direct comparisons are not just critical for validation but also contribute to the interpretation of the experimental results. We also describe coarse-grained simulations to study the possibility and effectiveness of shock-induced, endothermic, volume-collapsing reactions; these simulations quantify how the various characteristics of the chemical reactions attenuate the propagating shockwave and provide key information to experimentalists designing and synthesizing such materials.

8.1 Introduction

Shock or dynamical loading of a material causes a sudden increase in pressure and temperature which, in turn, triggers a wide range of processes through which the shocked material relaxes after the insult. The response is often a combination of pro-

M. M. Islam · A. Strachan (✉)
School of Materials Engineering and Birck Nanotechnology Center, Purdue University, West Lafayette, IN 47907, USA
e-mail: strachan@purdue.edu

M. Cherukara
Center for Nanoscale Materials, Argonne National Laboratory, Argonne, IL 60439, USA

E. Antillon
UES Inc., Dayton, Ohio 45433, USA

N. Goldman (ed.), *Computational Approaches for Chemistry Under Extreme Conditions*, Challenges and Advances in Computational Chemistry and Physics 28,
https://doi.org/10.1007/978-3-030-05600-1_8

cesses including plastic deformation [1–3] to relax the uniaxial compression caused by the shock, stress-induced phase transformations [4, 5], and chemical reactions [6, 7]. The fast strain rates involved (approximately 10^9 1/s) and the extreme pressures and temperatures achieved make shocks an attractive means to study materials behavior not accessible otherwise and to study materials at extreme conditions. For example, some crystal structures of certain minerals like silica form only at extreme conditions but remain in a metastable state after unloading [8]; consequently, their presence provides unique information about planetary systems. In addition, the fast loading results in nonequilibrium states and can result in processes not observed under equilibrium of slow-loading conditions. For example, Ravelo and Levitas found "virtual melting" as a new stress relaxation mechanism [9].

In this Chapter, we focus on recent molecular-level simulations of shock-induced chemical reactions in two classes of materials that, at first sight, appear to be complete opposites but, upon further analysis, show remarkable similarities. Section 8.3 discusses reactive atomistic simulations of high energy density (HE) materials, that react exothermically leading to gaseous products which, under appropriate conditions, can turn a shock into a detonation. Section 8.4 discusses coarse-grained simulations to explore materials that can weaken shockwaves via endothermic, volume-collapsing reactions. In both cases coupling the shock excitation to the degrees of freedom (DoFs) capable of causing chemical reactions is a complex process and does not happen instantaneously. Actually, in some cases chemical reactions occur when the system has not fully relaxed and equilibrated locally after the passage of the shockwave. Thus, of the focus areas of this chapter is how the nonequilibrium states right behind the shock front and the kinetics associated with the chemical reactions affect materials response. Before discussing the various applications we provide, in Sect. 8.2, a brief introduction of the simulation methods utilized and the details of the simulations presented in Sects. 8.3 and 4. A recent review of molecular simulations of shock processes [10] provides additional details on simulation techniques, applications to nonreactive systems and tutorials to perform atomistic shock simulations online using nanoHUB [11] cloud computing.

8.2 Atomistic and Coarse Grain Simulations of Shocks

Molecular dynamics simulations describe the temporal evolution of a group of atoms by solving classical equations of motion, given in Hamilton's form by

$$\dot{r}_i = v_i$$
$$\dot{v}_i = \frac{f_i}{m_i}$$

where $\{r_i\}$, $\{v_i\}$, and $\{f_i\}$ are the set of all atomic positions, velocities, and forces and $\{m_i\}$ atomic masses. In the absence of external fields, the forces originate from

atomic interactions and are obtained as the negative gradient of the total potential energy with respect to atomic positions.

Given initial conditions (atomic positions and velocities), the simulation predicts, in a deterministic manner, the temporal evolution of the system. When a group of atoms is evolved in time with realistic interactions, that include anharmonicities, the equations of motion take the system toward thermodynamic equilibrium; absent external perturbation the system will satisfy Maxwell–Boltzmann statistics. It is important to emphasize that while thermodynamic equilibrium is achieved under the appropriate conditions, it is not assumed in the simulation and nonequilibrium processes are captured explicitly.

8.2.1 Nonequilibrium Simulations of Shock Loading

Nonequilibrium shock simulations are often set up as an impact simulation between the previously equilibrated target and piston systems, both described in atomistic detail. The initial condition for such simulations is obtained by adding the desired impact velocity to the atoms in the target over the thermal velocities. It is common practice to zero the c.m. velocity of the entire system to avoid an overall translation of the systems within the simulation cell. Almost invariably, periodic boundary conditions are imposed in the cross-sectional directions; this mimics the response of a section of the material of interest away from the lateral free surfaces (far enough that the waves caused by the lateral expansion do not reach the section of interest during the simulated time).

With such initial conditions, the dynamical evolution of the system is described with adiabatic MD simulations (constant energy, number of atoms and volume or NVE ensemble). The passage of the shock leads to both the compression and heating of the shocked material and, as discussed above, can result in a plethora of materials responses to the extreme loads. Shock fronts are locally very sharp (a few atomic distances) and, thus, materials experience fast deformation and heating rates. These fast rates, in turn, lead to nonequilibrium thermodynamics states that do not satisfy equipartition of energy. As will be discussed below, this lack of equilibrium can affect processes triggered at or near the shock front.

8.2.2 Simulating Shock States Using Equilibrium MD

The main advantage of nonequilibrium shock simulations is that the shock front is described explicitly and the material experiences the ultrafast loading rates characteristic of shock loading, including the lack of local thermal equilibrium. An important drawback of such simulations is that the timescales achievable are approximately limited by the time it takes the shock to travel through the sample since a rarefaction wave moving back into the sample will be generated when the shock meets a free

surface. Consider a shock wave propagating through a sample of length L and a speed u_p; for a typical velocity of 5 km/s or 5 nm/ps, a simulation cell 100 nm is length will be traversed in only 20 ps. That is, the regions near the impact would have been in the shock state for only 20 ps when the rarefaction wave starts moving in. Extending the simulation a factor of n, requires increasing the simulation cell length by the same factor, resulting in an n^2 increase in computational cost (assuming a linear increase in cost with system size). In order to address this issue and enable longer simulation times for shocked systems, two methods have been proposed to simulate the state after the passage of a shock by modifying the equations of motion of the systems to compress and heat up the to the state corresponding to the shock state. Reed et al. proposed the MSST method [12] and Maillet, Ravelo, and collaborators proposed the Hugoniostat [13] described next.

For a steady-state shock with particle velocity u_p and shock velocity u_s, mass, energy and momentum conservation across the shock front result in the Rankine–Hugoniot jump conditions. These relate the unshocked state (density, energy, and pressure) with the shocked one. The Hugoniostat method uses a thermostat and a barostat to take the system from its initial state to the desired shock state for a given pressure. We note that this method can only be applied for single-wave situations, see [13, 14]. Multiple wave structures like in the case of plasticity following elastic loading should be simulated using different initial conditions for each wave.

8.2.3 Reactive MD Simulations

Shock-induced chemical reactions are important in applications ranging from explosives [15] to materials that can undergo volume-collapsing reactions that can be used for shock attenuation [16]. The development of reactive potentials over the last decades enabled the simulation of shock-induced chemistry. Here, we use ReaxFF [17, 18] to predict the decomposition and reaction of high energy density materials, Sects. 8.3 and 8.4. Building on earlier work [19], ReaxFF uses the concept of partial bond order between atoms to describe covalent interactions. These partial bond orders are many-body functions of the atomic positions and capture the character of the bonds (sigma, pi, double pi) and, importantly for MD simulations vary smoothly and approach zero as a bond is broken. All covalent terms, bond stretch, angles, and torsions depend on these bond orders which are also used to penalize over and under coordination. A second key element of ReaxFF is that electrostatic interactions are calculated using environment-dependent partial atomic charges obtained using electronegativity equalization method EEM [20].

8.2.4 Dynamics with Implicit Degrees of Freedom

While MD simulations are a powerful tool to explore dynamical loading, it is also computationally intensive and coarse grain models capable of capturing longer time and larger spatial scales are desirable for many applications. Here is use a particle-based coarse grain or mesoscale description, where particles describe group of atoms. Over the last decade or so, Strachan and collaborators have been developing the dynamics with implicit degrees of freedom (DID) family of methods to couple particle dynamics via MD with an implicit description of additional degrees of freedom. These implicit degrees of freedom can be atoms internal to the mesoparticles [21, 22], valence electrons [23] or an external electrochemical potential [24, 25].

In Sect. 8.4, we use DID to explore the possibility of volume-collapsing chemical reactions to weaken shockwaves with the objective of developing materials for protection against high-velocity impact or blasts. Particles represent a single molecule or small group of molecules that can undergo a stress-induced chemical reaction. In order to describe the average effect of the degrees of freedom internal to the particles, we include two internal variables to the mesoparticles: (i) an average particle radius to describe the volume collapsing chemistry and (ii) the average temperature of the remaining internal degrees of freedom. The dynamics of the average molecular radii is described via the Hamiltonian of the system. As described in Sect. 8.5, we add a potential energy term that captures how the energy of the molecules depends on their radius; a two well potential is used to describe the stress-induced phase transformation. The dynamics of the particles and their average radii is governed by the following Hamiltonian [26, 27]:

$$H = \sum_{i<j} \phi_{\text{inter}}\left(\vec{r}_j - \vec{r}_i - \sigma_j - \sigma_i\right) + \sum_i \phi_{\text{intra}}(\sigma_i) + \sum_i \frac{p_i^2}{2m_i} + \sum_i \frac{\pi_i^2}{2m_i^*}$$

where σ_i and π_i are the average molecular radius and momentum associated with particle i. Interactions between particles are described with a two-body potential, ϕ_{inter}, that depends on the distance between the particle surfaces. The dynamics of the particle's average radii is governed by an intramolecular potential, ϕ_{intra}, the details of which will be discussed in Sect. 8.4.

The internal degrees of freedom not described by the radii, are described in an average manner and their state is governed by the internal temperature of each mesoparticle, that evolves in time using DID equations of motion by exchanging energy with the local particles [27]:

$$\dot{T}_i^{\text{int}} = \nu_{\text{meso}} \frac{T_i^{\text{meso}} - T_i^{\text{int}}}{m_i C_i^{\text{int}} \langle \omega_{\text{inter}}^2 \rangle \Theta_0} \left| F_i^{\text{inter}} \right|^2 + \nu_{\text{rad}} \frac{T_i^{\text{rad}} - T_i^{\text{int}}}{m_i^* C_i^{\text{int}} \langle \omega_{\text{rad}}^2 \rangle \Theta_0} \left| F_i^{\text{rad}} \right|^2$$

where C_i^{int} is the specific heat associated with the internal DoFs, ν_{meso} and ν_{rad} describe the strength of the internal to intermolecular coupling and the internal to

radial coupling, respectively. Θo is a reference temperature, and the ratio $\frac{|F_i^{\text{rad}}|^2}{m_i^* \langle \omega_{\text{rad}}^2 \rangle}$ provides a natural timescale for the corresponding interaction.

Note that energy flow between internal DoF and the particles is determined by the relative local temperatures. If the local particle temperature around particle i is larger than its internal temperature, the particles are slowed down and the extra energy is captured by the internal DoF. Lin et al. [23] provides a detailed description of DID including its foundation on statistical mechanics. As described there, key features of the method include: (i) total energy and linear momentum are conserved; (ii) Galilean invariance; (iii) correct description of an isolated particle moving in free flight.

8.3 Shock-Induced Chemistry in High Energy Density Materials

The ultrafast loading rates associated with shock propagation in materials can reveal aspects of material behavior and properties that are inaccessible otherwise. Such nonequilibrium states include metastable phases [28], defect nucleation and multiplication [29] and of particular relevance to this section, nonequilibrium chemical reaction pathways [30]. In general, the process of shock loading a material, triggers a series of material responses that seek to minimize the potential energy in the system and alleviate the extreme shock-induced conditions of pressure and temperature. Such material responses include plastic deformation [1], phase transitions [31], and conformational changes in the case of organic crystals [32]. In each of these, the material response weakens the shock, as energy from the compressive wave is diverted to plastically deform the material, drive the material over a phase change or change the molecular conformation. Another mechanism triggered by shocks, that is the subject of this section, is chemical reactions. However, unlike the other mechanisms discussed above, not always does this result in a weakening of the shock. In HE materials, shock loading can trigger a series of net-exothermic reactions that form gaseous products. The exothermicity and volume expansion strengthens the shock, accelerates the chemistry and leads to a detonation if the chemical wave catches up with the shock wave. In a detonation, the wave propagation velocity (chemical and mechanical waves overlap) depends only on chemical kinetics and is consequently, independent of the initial piston velocity.

Experimental characterization of all shock-related phenomena is extremely difficult due to the short spatio-temporal length scales involved (from nm to microns and from ps to ns), but the problem is exacerbated when chemical reactions that are induced or assisted by the shock need to be taken into account. Recent progress on ultrafast spectroscopy coupled to laser shocks [33–37] is providing an unprecedented picture into chemistry at extreme conditions. Despite the impressive results, these experiments are not without limitations. For example, it is difficult to perform peak assignment in spectroscopic studies at extreme conditions. Thus, we believe only the combination of experiments and atomistic simulations will provide a definite descrip-

tion of the detailed chemistry of HE materials at extreme conditions. Interestingly, computational capabilities and models have matured to the point where it is possible to simulate large enough system sizes with accurate interatomic potentials, that can capture complex chemical reactions under nonequilibrium conditions [38]. In this section, we discuss shock-induced chemistry of poly vinyl nitrate, a high-energy amorphous polymer, and compare the predictions with ultrafast spectroscopy. Following the discussion of decomposition of a homogeneous, amorphous polymer we discuss recent results on the coupling of a shock wave with microstructural defects, the formation of hotspots and their criticality.

8.3.1 Atomistic Modeling of Shocks in HE Materials

Modeling a complete detonation from the initial chemical events to a detonation wave with all atom simulations remains beyond the scope of current computational capability. However, reactive MD simulations have provided unique insight into several aspects of the shock to detonation cycle, including the initial chemical reactions, and the role of preexisting material defects in the creation of hotspots.

Limited by the computational resources of the time, early MD work that studied reactive chemistry was based on the so-called AB system, a simplified representation of explosives, where diatomic AB molecules transform into A_2 and B_2 [39]. More recently, large-scale atomic simulations (up to ~36 million atoms) using a similar monoatomic model for nitrocubane, showed for the first time how hotspots can spontaneously form in a homogeneously heated sample, and how "critical" hotspots transition into a spherical detonation [40]. When a hotspot is formed, a competition arises between heat conduction away from the hotspot and accelerated kinetics due to the elevated temperatures. Smaller hotspots that have a larger surface area to volume quench, while larger hotspots can become self-sustaining giving rise to a deflagration wave that could eventually transition to a detonation. In their study, Hu et al. [40] found that for nitrocubane hotspots that reach a critical radius of ~1.5 nm continue to grow with a radial velocity that becomes supersonic. Figure 8.1 shows snapshots from the simulation, where only N_2 molecules are shown. A multitude of hotspots form spontaneously during the initial stages (Fig. 8.1a), most of which quench due to thermal conduction away from the hotspot, while a few larger ones become self-sustaining, eventually reaching supersonic velocities (Fig. 8.1d).

The presence of material defects have long been thought to play an important role in the initiation of chemistry and subsequent detonation, and the presence or absence of defects can have strong repercussions on the sensitivity of an explosive. For instance, the shock strengths required for the detonation of single-crystal explosives are significantly higher than shocks required to detonate granular powders [41]. Defects in the material such as voids, interfaces, or dislocation localize the energy from the shock through material jetting and shear into hotspots [42]. As with thermal hotspots, higher temperatures at hotspots lead to faster chemistry, which, in turn, increases the likelihood of a self-sustaining chemical wave [43].

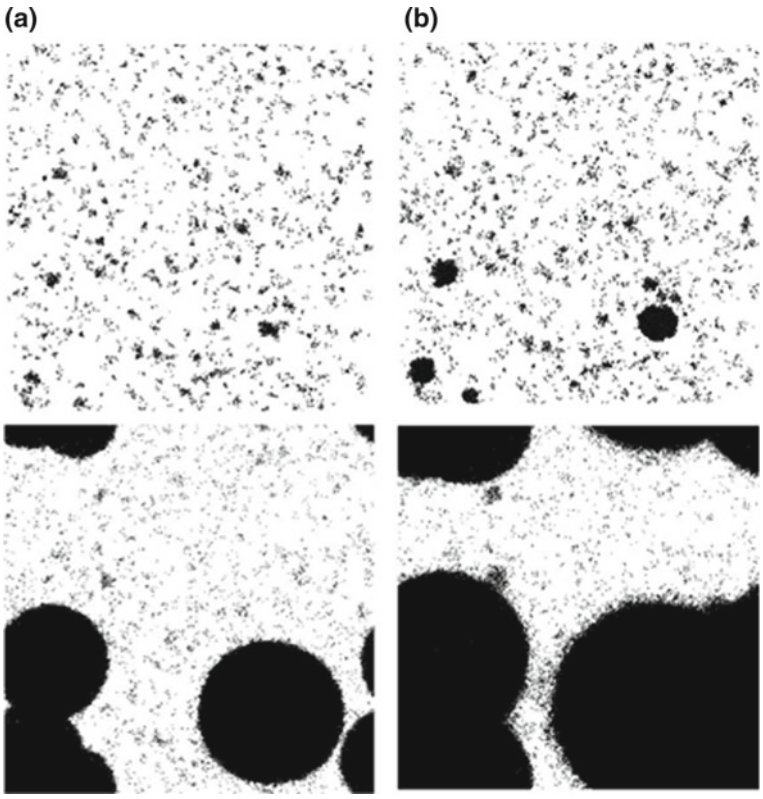

Fig. 8.1 Reaction progression during thermal cookoff of nitrocubane initially at 1160 K leading to the formation of N_2. Only N_2 molecules are shown for clarity. Times are **a** 5.0 ps, **b** 7.3 ps, **c** 11.4 ps, and **d** 13.2 ps. Reproduced with permission from [40]. Copyright (2011) American Chemical Society

Early MD work by Holian at Los Alamos and others, using a nonreactive LJ potential [44], showed significant temperature increase at the far wall of a collapsing void. The authors attributed this localized heating to recompression of rarified ejecta at the far wall of the pore, observing that the temperature increase in the collapsed pore scales with void size, but only up to a point [44]. A few years later, Herring et al. used the AB model to perform one of the first atomistic simulations of a shock to detonation transition [45]. Figure 8.2 shows the evolution of a shocked sample of the model material that initially contained a void of radius 5 nm. Atoms are colored by the nature of their bond, reactant AB molecules are in blue, products A_2 and B_2 are in green, while red atoms denote free radicals, i.e., isolated A or B atoms. Figure 8.2a shows a snapshot at an early stage, soon after the collapse of the void, where a deflagration wave starting from the collapsed void can be seen on the far left (region in green). Subsequently, more hotspots are seen to develop between the deflagration wave from the collapsed pore and the shock front (Fig. 8.2b). Finally,

Fig. 8.2 MD snapshots of a shock to detonation transition in a model AB explosive with a 5 nm radius void shocked at $U_p = 4$ km/s. Shock travels from left to right. Blue atoms denote unreacted material, green atoms represent product molecules while red atoms are unbonded monoatomic species. Snapshots show **a** Collapse of a void and the formation of a deflagration wave, **b** formation of hotspots between the deflagration wave and the shock front that ultimately give rise to a detonation (**c**). Reproduced with permission from [45]. Copyright (2010), American Physical Society

Fig. 8.2c shows the formation of a detonation wave that is separated from the original deflagration wave.

8.3.2 Shock-Decomposition of Poly Vinyl Nitrate (PVN)—MD Versus Experiments

In this section, we discuss the direct comparison of shock-induced chemistry between MD simulations and experiments. As discussed above, the microstructure in plastic-bonded HE systems plays a key role in localizing the energy of the shockwave in hotspots and in initiation. Such processes invariably complicate comparisons between experiments and MD simulations. We believe that homogeneous materials, including liquid and amorphous materials [46–48] are better choices for such direct comparisons.

PVN is, a homogeneous amorphous energetic polymer, used as a binder material. McGrane et al. [33] used ultrafast IR spectroscopy on laser-shocked PVN over a range of shock pressures and observed chemical reactions in 100s of picosecond timescales when shocked above a threshold of 18 GPa. The spectra reveal chemical reaction initiation via the disappearance of the NO_2 group stretching frequency; however, the limited spectral range of the experiments did not enable the characterization of detailed chemistry. A definitive understanding of the shock-induced chemistry of PVN requires a synergistic combination of experimental and computational studies, where experiments validate simulations and simulations help interpret experimental findings. We carried out shock simulations of PVN to establish a one-to-one comparison of the mechanical and chemical response of the material with the laser shock experiments; these results appeared in [49].

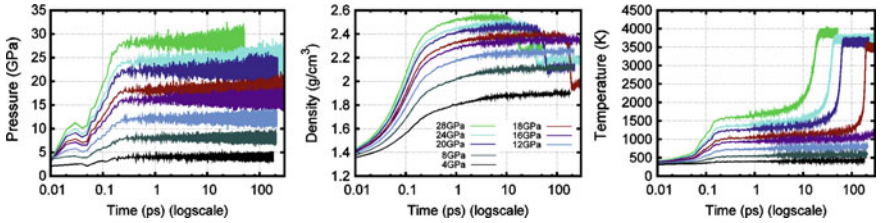

Fig. 8.3 Evolution of pressure, density, and temperature during shock simulations at various pressures. The sudden decrease in density and increase in temperature is indicative of the rapid chemical reactions

8.3.2.1 Shock Loading of PVN

A bulk amorphous PVN geometry at a density of 1.33 gm/cm^3 and molecular weight of 17806 gm/mol was used for the study. The shock simulations were performed utilizing Hugoniostat [13]-based MD simulation method. During shock loading, the uniaxial compression heats up the system to the final desired shock states. The ReaxFF-2014 force field [50] was used for all the simulations. The evolution of the thermodynamic properties such as pressure, density, and temperature was recorded from the shock simulations, and their temporal evolution is shown in Fig. 8.3. The applied rapid strain rate is representative to the shock process. The figures exhibit that the thermodynamic quantities were evolved to their final shocked states within around 1 ps. The applied compressive loading increases the system temperature, and for strong shock pressures, the system undergoes a rapid increase in volume and temperature followed by an induction period. The induction period is contingent on the applied shock and decreases with the increasing pressure. At 18 GPa shock pressure, the simulation-predicted induction time (~180 ps) is in good agreement with McGrane et al. [33] data. The rapid decrease in the density, that is, the increase in the volume is due to the exothermic reactions generated gaseous species.

The pressure–density and temperature–density data were derived from the simulations and shown in Fig. 8.4a, b. Since explosive materials produce gases upon exothermic reaction, that is, at a given pressure–temperature state, the products are less dense than the reactants, as such the products Hugoniot lies above the unreacted Hugoniot in the P, ρ space. The unreacted Hugoniot dictates the state from which the rapid chemical reactions start. It can be seen that both P-ρ and T-ρ plots have two regimes: unreactive Hugoniot for a relatively weak loading and reactive Hugoniot due to the exothermic volume-expanding reactions. The ReaxFF simulations nicely capture the shock pressure at which transition occurs and is in excellent agreement with McGrane et al. [33] reported data. The exothermic chemistry caused the system temperature to increase up to approximately 2000 K.

The Hugoniot relations [14] were used to calculate shock and particle velocity values. The data is presented in Fig. 8.4c along with the unreactive experimental [51] results. The reaction products Hugoniot regime exhibit a sudden increase in the shock velocities. The trend of a rapid increase of shock velocities at the onset

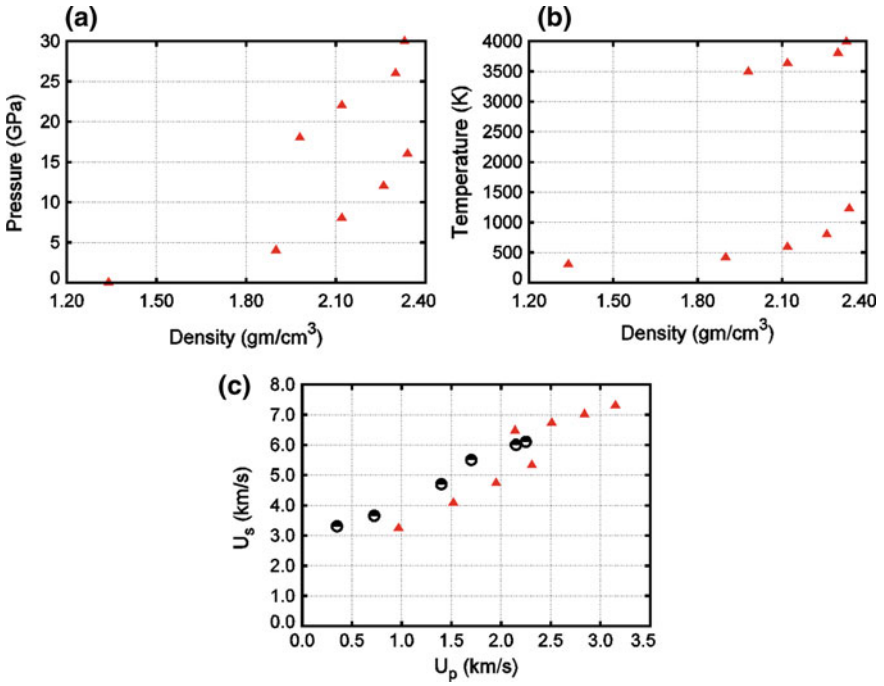

Fig. 8.4 Plot of unreacted and reaction products Hugoniots in **a** P-ρ, **b** T-ρ space, the product Hugoniots lies above the unreacted Hugoniots, **c** shock versus particle velocity data and comparison with the experimental results [51] (black half-filled circles)

of rapid reactions has also been observed in nitromethane shock experiment [52]. ReaxFF-2014 slightly underestimates the experimental unreactive u_s–u_p data. The simulation exhibit a transition to rapid exothermic chemistry at u_p= 2.2 km/s and u_s= 6.5 km/s. The sound speed (value of u_s at $u_p = 0$) computed from the simulations is 1.75 ± 0.05. This value is relatively smaller compared with the experimental data [51] of 3.2 ± 0.3 km/s.

8.3.2.2 Vibrational Analysis and Comparison with Shock Spectroscopy

In order to validate the ReaxFF simulations of shock-induced chemistry in PVN against the ultrafast spectroscopic experiments in a direct manner, we compute the time evolution of the vibrational density of states from the Fourier transform of atomistic velocities in the reactive MD simulations. The signature peaks of the various chemical groups and their evolution during the shock simulations provide key information about the reaction mechanisms and the associated time scales. The predicted time-resolved spectra at a shock pressure of 18 GPa is shown in Fig. 8.5. The NO_2-stretching frequency can be considered as an indicator of the rapid chemical

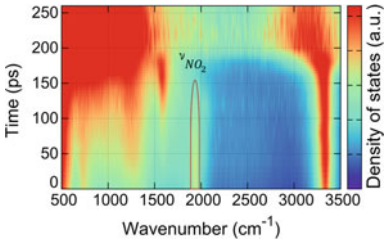

Fig. 8.5 Predicted time-resolved full spectra at 18 GPa shock simulation. The disappearance of NO_2 stretching frequency at ~150 ps is indicative to the onset of rapid chemical reactions

decomposition of the PVN. The figure demonstrates the disappearance of nitro group stretching mode (at ~1900 cm^{-1}) at a time-scale of around 150 ps; this marks the beginning of rapid exothermic chemistry, see Fig. 8.3. This predicted time scale is in excellent agreement with the McGrane et al. [33] reported experimental spectra of shocked PVN at 18 GPa. Furthermore, the calculated spectra yield important information about the evolution of the various intermediates. For example, a peak at 1600 cm^{-1} starts to develop in the spectra at about 50 ps and completely disappears at ~200 ps. The spectra calculated for the individual intermediates and the species analysis during the shock simulations show that the characteristic frequency corresponds to the NO. Thus, spectra capture the entire NO evolution history. Overall, the results demonstrate that the simulation-predicted spectra can help to unravel the experimental spectra to illustrate various reaction initiation mechanisms and related timescales.

8.3.3 Shock to Deflagration Transition and the Role of Hot Spots

While the studies described in Sect. 8.3.1 in model systems provided a wealth of information into the formation and criticality of dynamical hotspots, their simple nature can hide key aspects of the processes that operate in real HE materials where complex inter- and intramolecular processes are known to play key roles in the initiation of chemistry. As described earlier in the chapter, ReaxFF simulations can provide an accurate, all-atom description of the mechano-chemistry in a variety of nitramines [7, 53]. The prohibitive factor until recently has been the vastly greater computational cost ($10\times - 100\times$) as compared to the reduced models. In recent years, however, several research groups have performed multimillion atom ReaxFF simulations on state-of-the-art computational clusters to study hotspot formation resulting from material inhomogeneities such as voids [54] and the interfaces of polymer-bonded explosives [55].

More recently, using large-scale ReaxFF simulations, Wood et al. [30] provided the first atomic picture of a shock to deflagration transition in RDX using a realistic potential. They observed a crescent-shaped hotspot following pore collapse, that eventually gives rise to a deflagration wave. The authors observed three distinct

stages in the formation of the deflagration wave from the hotspot; in the first stage (up to ~10 ps from the collapse of the pore), the initial crescent-shaped hotspot that is formed grows until it is ~5 nm in width. Immediately following impact of ejecta with the far wall of the pore, the molecular center of mass temperature (T_{com}) and the molecular vibrational temperature or internal temperature (T_{vib}) of the impacted molecules differ greatly (T_{com} ~ 4000 K and T_{vib} ~ 1500 K at t_0). During the first stage of reaction, these temperatures equilibrate as energy is transferred from the molecular COM degrees of freedom to internal degrees of freedom. Surprisingly, within this short period, a few product molecules are also seen to form (Fig. 8.6).

During the second stage of reaction (~10–25 ps), the initial, crescent-shaped hotspot grows at a rapid rate, faster into the amorphous ejecta within the pore as compared to the crystalline material ahead of the pore. During this stage, the temperature within the growing hotspot reaches a steady-state value of ~4000 K and two distinct reaction fronts are seen, each with a surprisingly narrow width of ~5 nm. The third and final stage as described by the authors involves the steady-state growth of these reaction fronts at ~250 m/s.

A further surprise from their study was that thermal hotspots that they engineered to have the same temperature distribution, pressure, and morphology as the dynamically created hotspots showed much slower kinetics than the dynamic hotspot, suggesting that nonequilibrium effects arising from the mechanical impingement and shear of molecules during pore collapse, plays a vital role in accelerating the kinetics.

8.4 Shock Energy Absorption via Volume-Reducing Chemical Reactions

Section 8.3 focuses on HE materials where a shock can unleash exothermic, volume expanding reactions that can cause a detonation. In this section, we focus on exploring the possibility of using endothermic, volume collapsing chemistry to weaken a shockwave. The motivation of this effort is to contribute to the design of shock wave energy dissipation (SWED) materials that can be used for protection such as in traumatic brain injury [56] from impact and blast [57–61]. Our goal is to characterize how the details of the chemistry (enthalpy of formation, amount of volume reduction and kinetics) affect the ability of the material to weaken a shockwave. Since we are interested in general aspects of the problem and not in the detailed chemistry, we developed a coarse-grained model to describe SWED materials and characterize what features of its chemical reactions have the largest effort on shock attenuation.

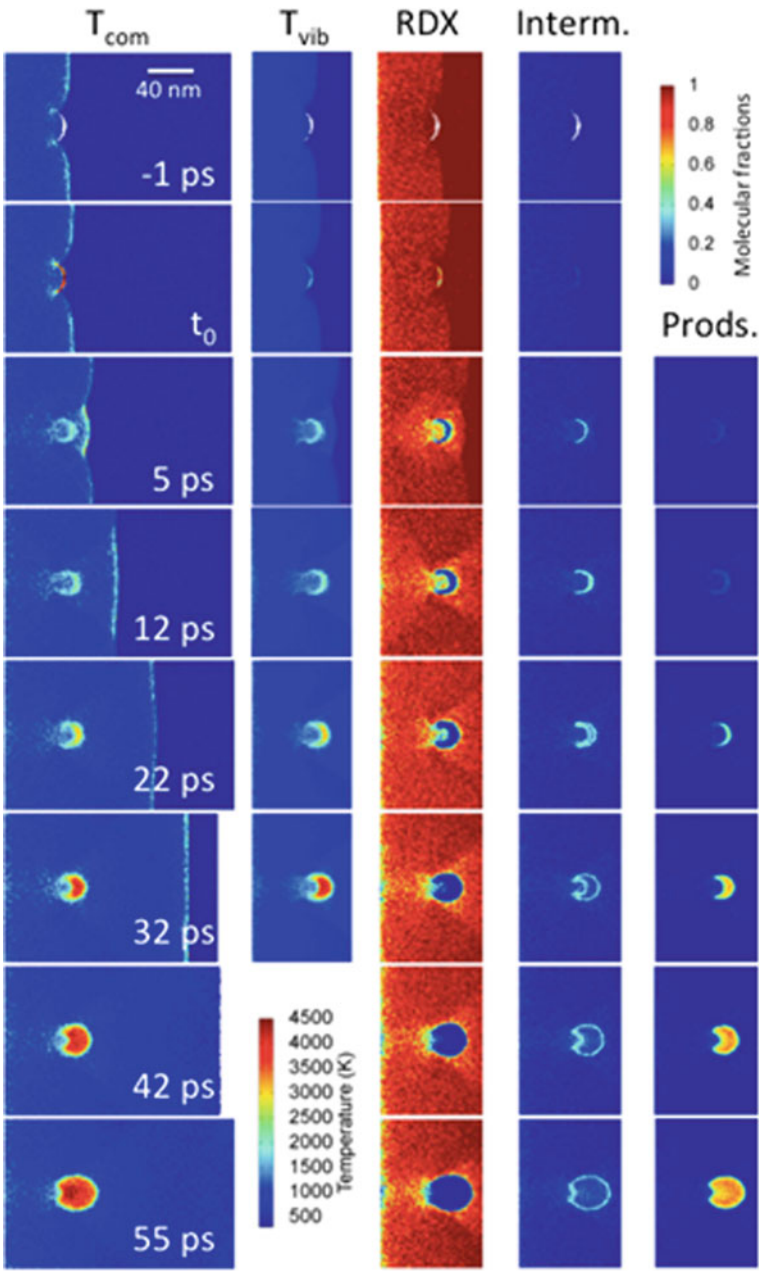

Fig. 8.6 Center of mass molecular temperatures (T_{com}), molecular vibrational temperatures (T_{vib}) and fractions of unreacted RDX, fractions of intermediate species, and fractions of final products at different stages. Reproduced with permission from [27]. Copyright (2015) American Chemical Society

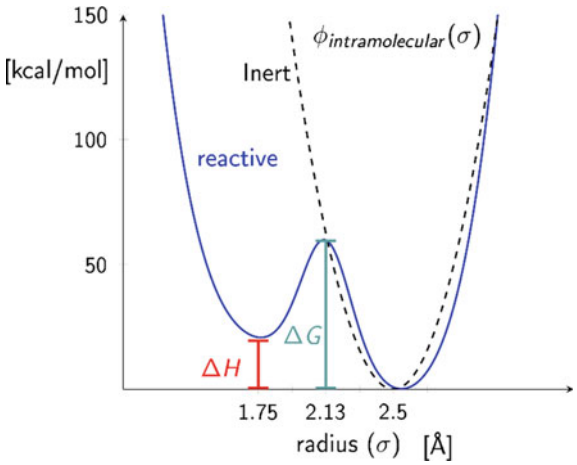

Fig. 8.7 Intramolecular potential for an inert and reactive materials as a function of the coarse-grained particle radius. For the reactive function, the initial state has a radius of size of 2.5 A while the final states are equal to 1.75 A; this corresponds to a 35% volume collapse. The final state can have a variable endothermic state ($\Delta H > 0$) an activation barrier $\Delta G > \Delta H$. The inert case is described by a harmonic potential with a stiffness that yields material properties close to molecular crystals such as HMX and Anthracene

8.4.1 A Family of SWED Materials

As described in Sect. 8.2, ChemDID provides a coarse-grained description of intramolecular chemistry via a potential energy function that controls the dynamics of the average radius of the particles. The potential energy shown in Fig. 8.7, was designed to describe endothermic, volume reducing reactions. This model entertains a specific type of chemistry proceeding via an order parameter (particle size) to transition from a low-energy high-volume state to a high-energy low-volume state. The key characteristics of the chemistry are: (i) endothermicity that we will vary between 0 and 30 kcal/mol, (ii) the volume reduction that varies from 10 to 65%, and (iii) the activation barrier from 0 to 100 kcal/mol.

The interaction between mesoparticles is described using the Morse potential (two exponentials) with distances measured from the surfaces of the particles, i.e., taking into account their radii, see [27]. The parameters of the two-body potential were chosen to result in density and stiffness comparable to HMX-molecule. The initial condition for the simulations consist of a target made of an FCC crystal with a lattice parameter $a = 10.1$ A and a molecular mass of $m = 296.1$ g/mol, which yields a density of 2.0 g/cm^3; this is close to the density of a molecular crystals such as HMX-molecule 1.9 g/cm^3. The system consists of 320,000 molecules with 200 lattice units in the z-directions and 20 lattice units along the x- and y-directions. Periodic boundary conditions are imposed along the x- and y-directions, while the z-direction has free surfaces. In order to follow the precise energy exchange between

the intra- and intermolecular DoF, we use an NVE ensemble where the system has been previously thermalized at 300 K and zero pressure.

8.4.2 Shock Loading and Energy Dissipation

The sample is impacted with a thin (one lattice constant thick), rigid and infinitely massive piston traveling at a constant speed in the z-direction. The infinitely massive piston does not slow down due to the interactions with the target, nor rarefaction waves are generated from its free surface. Thus, this setup generates a sustained shock where the piston does not slow down but it moves at a constant speed.

While in an inert material, plastic deformation or phase transformations are the only mechanisms that allow for stress relaxation, in a SWED material volume-reducing chemical reactions can significantly reduce pressure build up and attenuate the leading shock wave. The material under stress will attempt to deform or rearrange in order to alleviate its local stress build up. The material that is in its immediate proximity will quickly approach the same velocity and consequently this region experiences the largest strains rates where chemical reactions start to nucleate. As the piston is driven into the sample, a two-wave structure emerges separating a chemical region from the plastic region. Above a critical strain rate (HCL discussed below), a chemical region close to the piston nucleates and grows at a speed U_c, followed by a plastic regime growing at speed U_s; an elastic precursor to the plastic wave is present but it is negligible and very close in speed to the plastic wave, and therefore will be ignored for the rest of the discussion. Figure 8.8a shows the velocity profiles along the z-direction at various times after the piston impacts the target and Fig. 8.8b shows the pressure–volume (Hugoniot) curve representing the equation of state for the two regimes: one where both chemistry and plasticity nucleate (two-wave region), and one where only plasticity occurs (inert). The transition between the plastic regime and the chemical regime is denoted as the Hugoniot Chemical Limit (HCL). At extreme strains, the velocities of the chemical wave and the plastic wave will converge to the same value, and a single wave structure emerges, this is the overdriven regime.

The interplay between the various parameters playing a role in the kinetics of the model is discussed next.

In order to understand the roles that endothermicity, volume change, and the activation barrier have in the energy dissipation phenomena. We quantify the local pressure in both the inert and reactive parts of the Hugoniot in Fig. 8.9. Taking as a base case with an activation barrier $\Delta G = 30$ kcal/mol, volume change $= 35\%$ and endothermicity $\Delta H = 0$ kcal/mol. We see that increasing the activation barrier from $\Delta G = 30$ kcal/mol (red points) to 60 kcal/mol (blue points) will postpone the critical transition points (HCL) from about 7 to 17 Gpa, where a two-wave domain will persist at larger impact speeds until reaching the overdriven regime. Increasing the change in the volume collapse in the reactive material shifts the Hugoniot toward the left indicating a larger volume collapse. The pink points show the Hugoniot curve for

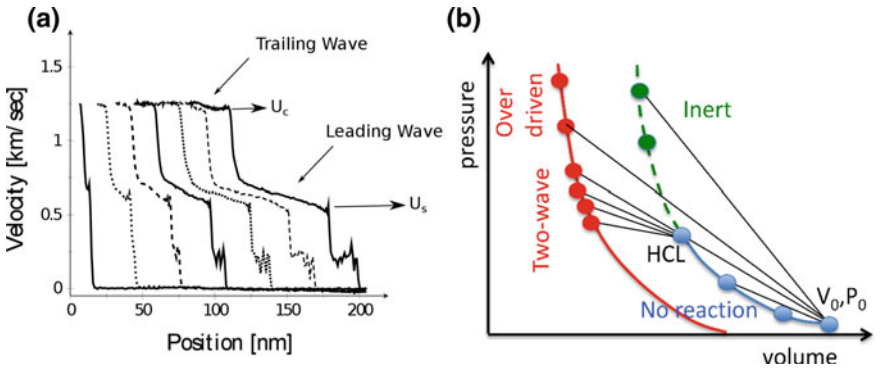

Fig. 8.8 **a** Progression of velocity profiles (in steps of 10 ps) showing the evolution of a leading wave traveling at speed U_s and a trailing wave (chemical wave) traveling at speed U_c. **b** A Hugoniot equation of state for reactive and inert materials. The transition from the inert-to-reactive is known as the Hugoniot Chemical Limit

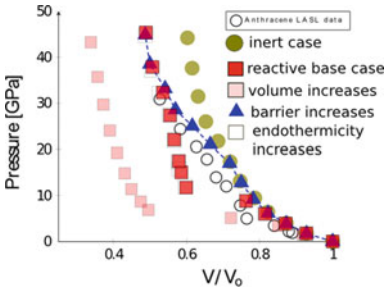

Fig. 8.9 **a** Hugoniot for various model materials for a range of piston speeds between $U_p = 0.25$ and 3.0 km/s (in steps of 0.25 km/s). The increase of volume collapse plays a major role in reducing the pressure until the Hugoniot state reaches the overdriven regime. In this regime, endothermicity only has a minor effect compared to a material with only volume-reducing properties. Larger activation barrier postpones the nucleation of chemical nucleation until larger impact speeds are accessible; For reference, experimental data on Anthracene is also shown

a volume change of 65% illustrating significant lower pressures in both the reactive and inert parts of the Hugoniot compared to the base case. The effect of endotrmicity was found to be null except for the overdriven regime. The empty symbols show a reactive material with endothermicity of $\Delta H = 30$ kcal/mol, which are consistent with the base case almost everywhere; in the overdriven regime, the pressures are lower but not significantly smaller.

In order to be have ideal shockwave absorbing properties, we argue that the HCL pressure needs to be as low as possible. This is because the plastic wave speed will travel at a fixed value in this two-wave regime independent of the impact speed of the piston and consequently its pressure will also be constant. Our model shows that the endothermicity plays a very weak role on the HCL, while the activation barrier and volume reduction both play a role in the HCL. Volume collapse lower than 20%

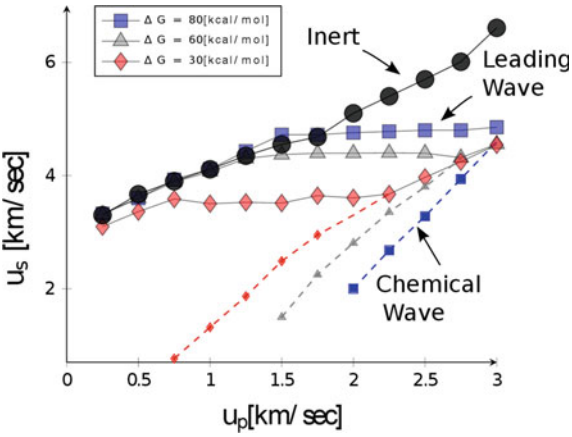

Fig. 8.10 Velocity of the shocked material (U_s) versus piston impact speed (U_p) for an inert material and three reactive materials with activation barriers between 30 and 80 kcal/mol. The chemical wave speed (U_c) is also shown in the dashed lines

are not expected at the molecular level, however, metal–organic frameworks (MOFs) can show larger volume collapse by breaking the ligands making up the structure leading to volume changes in the order of 60–80% [62].

The pressure in the shocked region can be related to the velocity of the shock wave by applying the Hugoniot–Rankine conditions.

$$P_s = \rho u_s \dot{x}_s$$

where ρ is the density of the unshocked material, u_s is the velocity of the leading shockwave, and $\dot{x}_s$ is the particle velocity. This last part can be shown to be a fraction of the velocity of the leading shockwave [27]. Hence, the pressure in the shocked region is a direct function of the shockwave velocity. Therefore, it is important to understand how chemical reaction can affect the shockwave velocity. At lower activation barriers, chemistry starts to nucleate earlier as a function of piston impact speed. Figure 8.10 shows the shock velocity of the leading wave (solid lines) and the chemical wave speed (dashed lines) versus the applied piston speed (U_p).

Above a critical impact speed, the HCL limits are reached, and a reactive region is able to grow at a steady rate. Chemistry nucleation helps to absorb the shock energy and helps to maintain the leading shockwave at a relatively constant speed. On the other hand, the inert case can only relieve stress through plastic deformations, and the shockwave velocity bends down slightly with piston speed until reaches the overdriven regime relatively early at about $U_p = 1.75$ km/s. The reactive model materials can postpone the overdriven regimes for the reactive materials after $U_p =$ 2.25, 2.75, and 3.0 km/s for $\Delta G = 30$, 60, and 80 kcal/mol, respectively. This shows that while rapid chemistry nucleation rate damps the shockwave energy the most, it ultimately arrives at the overdriven regime earlier.

In conclusion, endothermic, volume-reducing chemistry can weaken shockwaves [26, 27, 62, 63]. The role of endothermicity was found to be minimal while the volume-reducing contribution affects the damping the most. This study focuses on

sustained shockwaves, where the mass of the piston is assumed to be infinitely massive, and thus corresponds the extreme values expected during the collision with a finite piston. Once the local pressure comes down below the HCL, chemical reactions are not expected to nucleate and grow at larger scales. However, for the sizes considered in this study, the sustained wave simulations represent a realistic scenario of what might occur during the chemical reactions induced during shock loading conditions.

8.5 Conclusion and Outlook

This chapter focused on an atomic level and coarse grain studies of shock-induced chemistry. Initiating chemistry requires for the energy in the initial impact to be transferred into bond vibrations with characteristic lengths of Angstroms and vibrational periods on tens of femtoseconds (~10^{-14} s). In most solid HE materials, microstructural features like voids, grain boundaries, and cracks help localize the energy of the shock spatially into hotspots. At the same time, energy is localized in real space it needs to delocalize (or equilibrate) in the frequency domain. This is because, the macroscopic shock couples more strongly to long-frequency long-wavelength modes and inter- and intra-vibrational relaxation processes are responsible to locally equilibrate the system and transfer energy to high-frequency modes, this is called up-pumping [36]. A combination of large-scale atomistic simulations and recent experiments is providing unprecedented detail into these processes.

We described simulations playing various roles. On the one hand, detailed simulations about dynamical hotspots in RDX provide new insight into the reactivity of nanoscale hotspots. Specifically, we find that dynamically created hotspots are more reactive than counterparts with identical size and thermodynamic conditions by created under equilibrium conditions. On the other hand, coarse grain simulations can be used to help the design of new materials with the desired response of shock loading by relating how the characteristics of the chemical reactions affect shock propagation. Finally, first principles simulations have the potential to help the design of new materials with a reduced set of experiments, but the accuracy of its predictions must be rigorously quantified. We showed the emerging possibility of direct validation of predicted shock-induced chemistry against experiments. Ongoing efforts to achieve ultrafast, broadband spectroscopy in shock experiments will enable a better comparison and provide definite information about the detailed chemistry of HE materials under shock loading.

References

1. Holian BL, Lomdahl PS (1998) Plasticity induced by shock waves in nonequilibrium molecular-dynamics simulations. Sci 280:2085–2088
2. Bringa EM, Caro A, Wang Y et al (2005) Ultrahigh strength in nanocrystalline materials under shock loading. Sci 309:1838–1841
3. Chen MW, McCauley JW, Dandekar DP, Bourne NK (2006) Dynamic plasticity and failure of high-purity alumina under shock loading. Nat Mater 5:614
4. Duvall GE, Graham RA (1977) Phase transitions under shock-wave loading. Rev Mod Phys 49:523
5. Kadau K, Germann TC, Lomdahl PS, Holian BL (2002) Microscopic view of structural phase transitions induced by shock waves. Sci 296:1681–1684
6. Yang Y, Wang S, Sun Z, Dlott DD (2004) Propagation of shock-induced chemistry in nanoenergetic materials: the first micrometer. J Appl Phys 95:3667–3676
7. Strachan A, van Duin ACT, Chakraborty D et al (2003) Shock waves in high-energy materials: the initial chemical events in Nitramine RDX. Phys Rev Lett 91:098301. https://doi.org/10.1103/PhysRevLett.91.098301
8. Hirai H, Kondo K (1991) Modified phases of diamond formed under shock compression and rapid quenching. Sci 253:772–774
9. Levitas VI, Ravelo R (2012) Virtual melting as a new mechanism of stress relaxation under high strain rate loading. Proc Natl Acad Sci 109:13204–13207
10. Wood MA, Cherukara MJ, Antillon E, Strachan A (2017) Molecular dynamics simulations of shock loading of materials: a review and tutorial. Rev Comput Chem 43–92
11. Strachan A, Klimeck G, Lundstrom M (2010) Cyber-enabled simulations in nanoscale science and engineering. Comput Sci Eng 12:12–17
12. Reed EJ, Fried LE, Joannopoulos JD (2003) A method for tractable dynamical studies of single and double shock compression. Phys Rev Lett 90:235503. https://doi.org/10.1103/PhysRevLett.90.235503
13. Maillet J-B, Mareschal M, Soulard L et al (2000) Uniaxial hugoniostat: a method for atomistic simulations of shocked materials. Phys Rev E 63:016121. https://doi.org/10.1103/PhysRevE.63.016121
14. Ravelo R, Holian BL, Germann TC, Lomdahl PS (2004) Constant-stress hugoniostat method for following the dynamical evolution of shocked matter. Phys Rev B 70:014103. https://doi.org/10.1103/PhysRevB.70.014103
15. Bdzil JB, Stewart DS (2007) The dynamics of detonation in explosive systems. Annu Rev Fluid Mech 39:263–292. https://doi.org/10.1146/annurev.fluid.38.050304.092049
16. Yang K, Lee J, Sottos NR, Moore JS (2015) Shock-induced ordering in a nano-segregated network-forming ionic liquid. J Am Chem Soc 137:16000–16003
17. Van Duin AC, Dasgupta S, Lorant F, Goddard WA (2001) ReaxFF: a reactive force field for hydrocarbons. J Phys Chem A 105:9396–9409
18. Senftle TP, Hong S, Islam MM et al (2016) The ReaxFF reactive force-field: development, applications and future directions. Npj Comput Mater 2:15011. https://doi.org/10.1038/npjcompumats.2015.11
19. Tersoff J (1988) New empirical approach for the structure and energy of covalent systems. Phys Rev B 37:6991
20. Mortier WJ, Ghosh SK, Shankar S (1986) Electronegativity-equalization method for the calculation of atomic charges in molecules. J Am Chem Soc 108:4315–4320. https://doi.org/10.1021/ja00275a013
21. Strachan A, Holian BL (2005) Energy exchange between mesoparticles and their internal degrees of freedom. Phys Rev Lett 94:014301
22. Lynch K, Thompson A, Strachan A (2008) Coarse grain modeling of spall failure in molecular crystals: role of intra-molecular degrees of freedom. Model Simul Mater Sci Eng 17:015007
23. Lin K-H, Holian BL, Germann TC, Strachan A (2014) Mesodynamics with implicit degrees of freedom. J Chem Phys 141:064107. https://doi.org/10.1063/1.4891308

24. Onofrio N, Guzman D, Strachan A (2015) Atomic origin of ultrafast resistance switching in nanoscale electrometallization cells. Nat Mater 14:440–446. https://doi.org/10.1038/nmat4221
25. Onofrio N, Strachan A (2015) Voltage equilibration for reactive atomistic simulations of electrochemical processes. J Chem Phys 143:054109. https://doi.org/10.1063/1.4927562
26. Antillon E, Banlusan K, Strachan A (2014) Coarse grain model for coupled thermo-mechano-chemical processes and its application to pressure-induced endothermic chemical reactions. Model Simul Mater Sci Eng 22:025027
27. Antillon E, Strachan A (2015) Mesoscale simulations of shockwave energy dissipation via chemical reactions. J Chem Phys 142:084108
28. Millot M, Dubrovinskaia N a, Černok A, et al (2015) Shock compression of stishovite and melting of silica at planetary interior conditions. Sci 347:418–420
29. Erhart P, Bringa EM, Kumar M, Albe K (2005) Atomistic mechanism of shock-induced void collapse in nanoporous metals. Phys Rev B 72:052104
30. Wood MA, Cherukara MJ, Kober EM, Strachan A (2015) Ultrafast chemistry under nonequilibrium conditions and the shock to deflagration transition at the nanoscale. J Phys Chem C 119:22008–22015. https://doi.org/10.1021/acs.jpcc.5b05362
31. Knudson MD, Desjarlais MP, Dolan DH (2008) Shock-wave exploration of the high-pressure phases of carbon. Sci 322:1822–1825
32. Dreger ZA, Gruzdkov YA, Gupta YM, Dick JJ (2002) Shock wave induced decomposition chemistry of pentaerythritol tetranitrate single crystals: time-resolved emission spectroscopy. J Phys Chem B 106:247–256
33. McGrane SD, Moore DS, Funk DJ (2004) Shock induced reaction observed via ultrafast infrared absorption in poly(vinyl nitrate) films. J Phys Chem A 108:9342–9347. https://doi.org/10.1021/jp048464x
34. Dlott DD (2011) New developments in the physical chemistry of shock compression. Annu Rev Phys Chem 62:575–597. https://doi.org/10.1146/annurev.physchem.012809.103514
35. Dlott DD (1990) Theory of ultrahot molecular solids: vibrational cooling and shock-induced multiphonon up pumping in crystalline naphthalene. J Chem Phys 93:1695–1709. https://doi.org/10.1063/1.459097
36. Dlott DD (1990) Shocked molecular solids: vibrational up pumping, defect hot spot formation, and the onset of chemistry. J Chem Phys 92:3798–3812. https://doi.org/10.1063/1.457838
37. Bassette WP, Dlott DD (2016) High dynamic range emission measurements of shocked energetic materials: Octahydro-1,3,5,7-tetranitro-1,3,5,7-tetrazocine (HMX). J Appl Phys 119:225103. https://doi.org/10.1063/1.4953353
38. Shan T-R, Thompson AP (2014) Micron-scale reactive atomistic simulations of void collapse and hotspot growth in pentaerythritol tetranitrate. In: 15th Int. Detonation Symp. Sandia National Laboratories (SNL-NM), Albuquerque, NM (United States), Albuquerque, NM (United States), p SAND2015–1243C
39. Brenner DW, Robertson DH, Elert ML, White CT (1993) Detonations at nanometer resolution using molecular dynamics. Phys Rev Lett 70:2174
40. Hu Y, Brenner DW, Shi Y (2011) Detonation initiation from spontaneous hotspots formed during cook-off observed in molecular dynamics simulations. J Phys Chem C 115:2416–2422
41. Marsh SP (1980) LASL shock hugoniot data. University of California Press
42. Cherukara MJ, Germann TC, Kober EM, Strachan A (2014) Shock loading of granular Ni/Al composites. Part 1: mechanics of loading. J Phys Chem C 118:26377–26386
43. Cherukara MJ, Germann TC, Kober EM, Strachan A (2016) Shock loading of granular Ni/Al composites. Part 2: shock-induced chemistry. J Phys Chem C 120:6804–6813
44. Holian BL, Germann TC, Maillet J-B, White CT (2002) Atomistic mechanism for hot spot initiation. Phys Rev Lett 89:285501
45. Herring SD, Germann TC, Grønbech-Jensen N (2010) Effects of void size, density, and arrangement on deflagration and detonation sensitivity of a reactive empirical bond order high explosive. Phys Rev B 82:214108
46. Campbell AW, Davis WC, Travis JR (1961) Phys Fluids 4(4):498

47. Bowden FP, Yoffe AD (1952) Initiation and growth of explosion in liquids and solids. CUP Archive
48. Field JE (1992) Hot spot ignition mechanisms for explosives. Acc Chem Res 25:489–496
49. Islam MM, Strachan A (2017) Decomposition and reaction of polyvinyl nitrate under shock and thermal loading: a ReaxFF reactive molecular dynamics study. J Phys Chem C. https://doi.org/10.1021/acs.jpcc.7b06154
50. Wood MA, van Duin AC, Strachan A (2014) Coupled thermal and electromagnetic induced decomposition in the molecular explosive αHMX: a reactive molecular dynamics study. J Phys Chem A 118:885–895
51. Moore DS, McGrane SD, Funk DJ (2004) Ultrafast spectroscopic investigation of shock compressed energetic polymer films. AIP Conf Proc 706:1285–1288. https://doi.org/10.1063/1.1780473
52. Brown KE, McGrane SD, Bolme CA, Moore DS (2014) Ultrafast chemical reactions in shocked nitromethane probed with dynamic ellipsometry and transient absorption spectroscopy. J Phys Chem A 118:2559–2567. https://doi.org/10.1021/jp4125793
53. Strachan A, Kober EM, van Duin AC et al (2005) Thermal decomposition of RDX from reactive molecular dynamics. J Chem Phys 122:054502
54. Shan T-R, Thompson AP (2014) Shock-induced hotspot formation and chemical reaction initiation in PETN containing a spherical void. In: J Phys Conf Ser, IOP Publishing, p 172009
55. An Q, Zybin SV, Goddard WA III et al (2011) Elucidation of the dynamics for hot-spot initiation at nonuniform interfaces of highly shocked materials. Phys Rev B 84:220101
56. Kulkarni SG, Gao X-L, Horner SE et al (2013) Ballistic helmets—their design, materials, and performance against traumatic brain injury. Compos Struct 101:313–331
57. Morinière FD, Alderliesten RC, Benedictus R (2014) Modelling of impact damage and dynamics in fibre-metal laminates—a review. Int J Impact Eng 67:27–38
58. Sadighi M, Alderliesten RC, Benedictus R (2012) Impact resistance of fiber-metal laminates: a review. Int J Impact Eng 49:77–90
59. López-Puente J, Arias A, Zaera R, Navarro C (2005) The effect of the thickness of the adhesive layer on the ballistic limit of ceramic/metal armours: an experimental and numerical study. Int J Impact Eng 32:321–336
60. Crupi V, Epasto G, Guglielmino E (2012) Collapse modes in aluminium honeycomb sandwich panels under bending and impact loading. Int J Impact Eng 43:6–15
61. Grujicic M, Pandurangan B, Bell WC et al (2011) Molecular-level simulations of shock generation and propagation in polyurea. Mater Sci Eng A 528:3799–3808
62. Banlusan K, Strachan A (2016) Shockwave energy dissipation in metal-organic framework MOF-5. J Phys Chem C 120:12463–12471. https://doi.org/10.1021/acs.jpcc.6b02283
63. Banlusan K, Antillon E, Strachan A (2015) Mechanisms of plastic deformation of metal-organic framework-5. J Phys Chem C 119:25845–25852